Сейсмостойкость сооружений

SEISMIC RESISTANCE

Influence of the concrete strength and the type of supports on the stress-strain state of a hyperbolic paraboloid shell footbridge structure

David Cajamarca-Zuniga[1,2] ✉, Sebastian Luna[1]

[1]*Catholic University of Cuenca, Cuenca, Republic of Ecuador*
[2]*Peoples' Friendship University of Russia (RUDN University), Moscow, Russian Federation*
✉ cajamarca.zuniga@gmail.com

Abstract. *Relevance.* This work is the first in a series of publications on the selection of a suitable analytical surface for implementation as a self-supporting structure for a thin shell footbridge. The study on the influence of concrete strength, live load position and support types on the stress-strain state of a hyperbolic paraboloid (hypar) shell is presented. *Objective* – to define the initial design parameters such as the appropriate concrete strength and the support type that generates the best structural behaviour to perform the subsequent structural design of a thin shell footbridge. *Methods.* The static finite element analysis was performed for 4 compressive strengths of concrete (28, 40, 80, 120 MPa) which correspond normal, high and ultra-high resistance concrete, 5 different live load arrangements and 3 different support conditions. *Results.* The shell model with pinned (two-hinged) supports shows the same vertical displacements as the model with fixed supports (hingeless). For the studied shell thickness, in terms of stress behaviour, the model with pinned ends is more efficient. The combination of two-hinged supports with 80 MPa concrete strength shows a better structural performance.

Keywords: finite element analysis, footbridge, hyperbolic paraboloid, shell structure, stress-strain state, high resistance concrete, ultra-high performance concrete

Влияние прочности бетона и типа опор на напряженно-деформированное состояние гиперболической параболоидной оболочки для конструкции пешеходного моста

Д. Кахамарка-Сунига[1,2] ✉, С. Луна[1]

[1]*Католический университет города Куэнки, Куэнка, Республика Эквадор*
[2]*Российский университет дружбы народов, Москва, Российская Федерация*
✉ cajamarca.zuniga@gmail.com

Аннотация. *Актуальность.* Работа является первой в серии публикаций по выбору аналитической поверхности, подходящей в качестве самонесущей конструкции оболочки для пешеходного моста. Исследуется влияние прочности бетона, положения нагрузки от толпы людей и типа опор на напря-

David Cajamarca-Zuniga, Associate Professor of the Department of Civil Engineering, Catholic University of Cuenca, Av. De las Americas & Humboldt, Cuenca, 010101, Republic of Ecuador, PhD postgraduate student, Assistant Professor of the Department of Civil Engineering, Engineering Academy, Peoples' Friendship University of Russia (RUDN University), 6 Miklukho-Maklaya St, Moscow, 117198, Russian Federation; ORCID: 0000-0001-8796-4635, Scopus Author ID: 57251506300, eLIBRARY SPIN-code: 6178-4383, Researcher ID: AAO-8887-2020; cajamarca.zuniga@gmail.com
Sebastian Luna, Civil Engineer, master student of the Department of Civil Engineering, Catholic University of Cuenca, Av. De las Americas & Humboldt, Cuenca, 010101, Republic of Ecuador; ORCID: 0000-0003-2431-3960; selunav07@est.ucacue.edu.ec

Кахамарка-Сунига Давид, доцент департамента строительства, Инженерный факультет, Католический университет города Куэнки, Республика Эквадор, 010101, Куэнка, Av. De las Americas & Humboldt, аспирант, ассистент департамента строительства, Инженерная академия, Российский университет дружбы народов, Российская Федерация, 117198, Москва, ул. Миклухо-Маклая, д. 6; ORCID: 0000-0001-8796-4635, Scopus Author ID: 57251506300, eLIBRARY SPIN-код: 6178-4383, Researcher ID: AAO-8887-2020; cajamarca.zuniga@gmail.com
Луна Себастиан, инженер-строитель, магистр Инженерного факультета, Католический университет города Куэнки, Республика Эквадор, 010101, Куэнка, Av. De las Americas & Humboldt; ORCID: 0000-0003-2431-3960; selunav07@est.ucacue.edu.ec

женно-деформированное состояние гиперболической параболоидной оболочки (гипар). *Цель* – определить исходные конструктивные параметры, такие как рекомендуемая прочность бетона и тип опоры, обеспечивающие наилучшее структурное поведение, для последующего выполнения расчета конструкции оболочки для пешеходного моста. *Методы.* Статический конечно-элементный анализ был проведен для четырех пределов прочности на сжатие бетона (28, 40, 80, 120 МПа), которые соответствуют нормальному, высокому и сверхвысокому сопротивлению бетона, пяти различным схемам расположения нагрузки от толпы и трем различным условиям опирания. *Результаты.* Двухшарнирные и бесшарнирные модели показывают одинаковые вертикальные перемещения. Для исследуемой толщины оболочки с точки зрения внутренних усилий двухшарнирная модель является более эффективной. Комбинация шарнирных неподвижных опор с прочностью бетона 80 МПа показала лучшее структурное поведение.

Ключевые слова: конечно-элементный анализ, пешеходный мост, гиперболический параболоид, оболочка, напряженно-деформированное состояние, высокопрочный бетон, ультравысокопрочный бетон

Introduction

Thin shells, as well as long-span structures, spatial grids, tensegrity systems, tall buildings, among other systems, are related to "special structures" [1]. Shells are form-resisting structures, as they mainly resist loads because of their form rather than the amount of their material (cross-section). Because of their special qualities, shells are used wherever high efficiency is required, such as to cover long spans with high resistance and minimum material [2]. Felix Candela fomented the surge of popularity of shell structures in the 1950s, and his works launched the modern shell era by attracting the attention of architects and structural engineers [1]. In 1951 Candela built a 11 m span and 15 mm thickness hyperbolic paraboloid shell in Mexico [3–5], what was an innovative project at these time. The Candela's built hyperbolic paraboloid shells show that was possible to minimise workforce and material resources [6]. Despite this, the widespread building of thin reinforced concrete shells ended abruptly at the end of the 1960s [7] and for many time the use of large span shell structures has lost its popularity compared to the peak of their construction in the 1950–1960s [8].

The 21st century brought a new era for architectural design [9] and improvement of 3D finite element analysis software. Nowadays, more architects and engineers are becoming interested in the design of long-span shell structures. Thus, the authors of this article set out to study the possibilities of using different analytical surfaces for the construction of a thin shell footbridge, where the shell is both the supporting structure and the walking surface.

The hyperbolic paraboloid (hypar) has been known in mathematics since the 17th century and first appeared in architecture at the end of the 19th century [3]. Mathematically synclastic surfaces have positive Gaussian curvature K, while the anticlastic (hyperbolic) surfaces have negative curvature K. Both synclastic and anticlastic surfaces are of double curvature. Double curvature surfaces, if properly restrained, can work only as membranes, irrespective of the applied loads. This singularity can be seen by comparing the failure of a cylindrical and spherical vaults under vertical loads; the first will fail in bending, the second in tension.

The hyperbolic paraboloid is a twice ruled surface of negative Gaussian curvature [10], and is categorized as an anticlastic surface [11]. This anticlastic ruled surface could be generated by straight lines. Therefore, this shell shaped structure is simpler to build [12; 13]. It is important to consider that the hyperbolic paraboloid shell may be stable in the postcritical range due to negative Gaussian curvature since there are also fibres in tension that stabilise the shell [14].

At present, there are few projects in which shells are used as supporting structures for bridges. Among the most notable projects are the Musmeci Bridge over the Basento river in Italy (Figure 1, *a*), the Matadero Bridge over the Manzaneros river in Spain (Figure 1, *b*) and the TRUMPF Bridge over Gerlinger Strasse in Germany (Figure 1, *c*).

The Musmeci Bridge is about 300 m long and is composed of a RC box-section deck supported by a RC continuous double-curvature shell. The shell forms 4 equal spans of 69.20 m each, has a thickness of 0.30 m and is characterised by deeper ribs at both sides [15]. The Matadero footbridge is a RC (40 MPa) sinclastic shell that supports a suspended metallic deck [16; 17], were the bearing structure is a shell with 43.50 m span, 8.40 m width, 7.70 m of rise and variable thickness from 0.15 m in the centre to 0.57 m in the supports [18]. The footbridge at TRUMPF headquarters is a double curved steel shell with 28 m span, 2.20 m width, and only 20 mm thickness [19]. It should be noted that only the last of the mentioned projects (Figure 1, *c*) uses the shell structure both as a load-bearing element and as a walking surface.
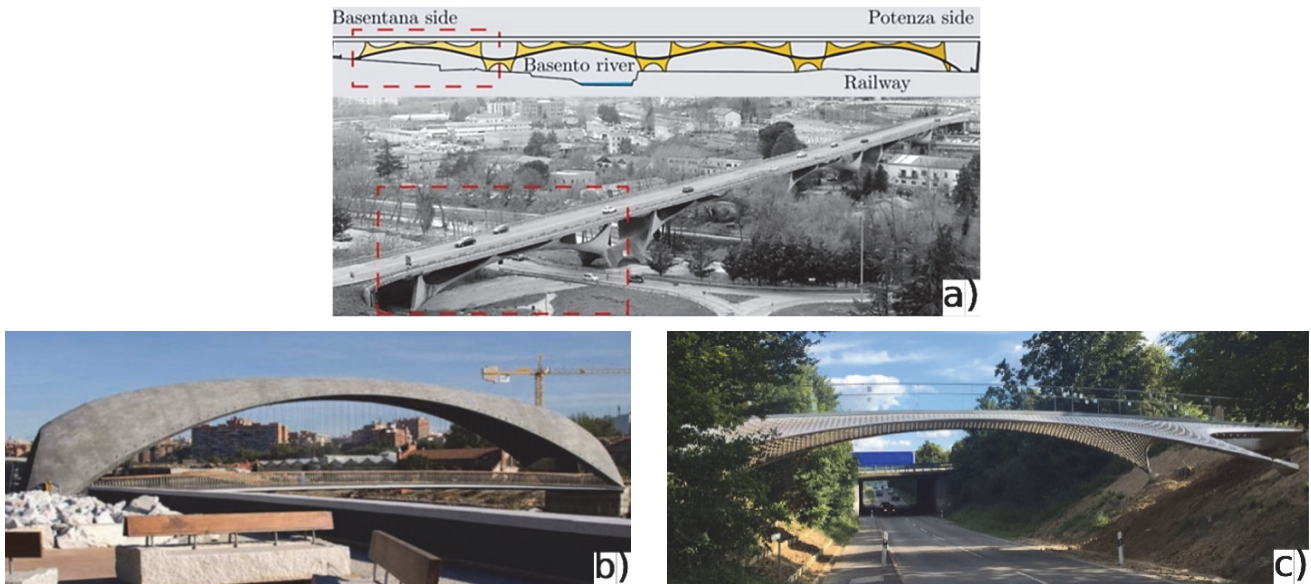
Figure 1. Musmeci's bridge, Potenza, Italy (*a*); Matadero footbridge, Madrid, Spain (*b*); TRUMPF footbridge, Ditzingen, Germany (*c*)

This research is the first stage of a project that performs a comparison of the static and dynamic structural behaviour, architectural influence and environmental impacts between a conventional-structured footbridge built in the city of Cuenca (Ecuador) and a proposed shell-shaped footbridge, where the shell is both the load-bearing element and the walking surface. The whole project will study the structural behaviour of different analytical surfaces (hyperbolic paraboloid, conoid, torse) to define the most suitable geometric shape for a pedestrian bridge. This article shows the results of the first stage of the cited research. In this stage, the stress-strain state of the proposed hyperbolic paraboloid bridge was determined. The results will allow us to establish the optimal type of supports and concrete strength for this type of structure in order to perform the subsequent structural design in the next stage. The issues of local stability of the shell on the upper edges, as well as the reinforcement of the shell as a whole and in different zones depending on the stress-strain state, are not considered in the present article.

Methodology

In the present work, we defined the overall dimensions of the studied shell according to the dimensions of an existing bridge built with a conventional structural system in the city of Cuenca (Ecuador). The Juana de Oro footbridge (Figure 2) is a three-hinged arch with $L = 24$ m of span, $B = 5$ m of width and $f = 1.2$ m of rise [20].
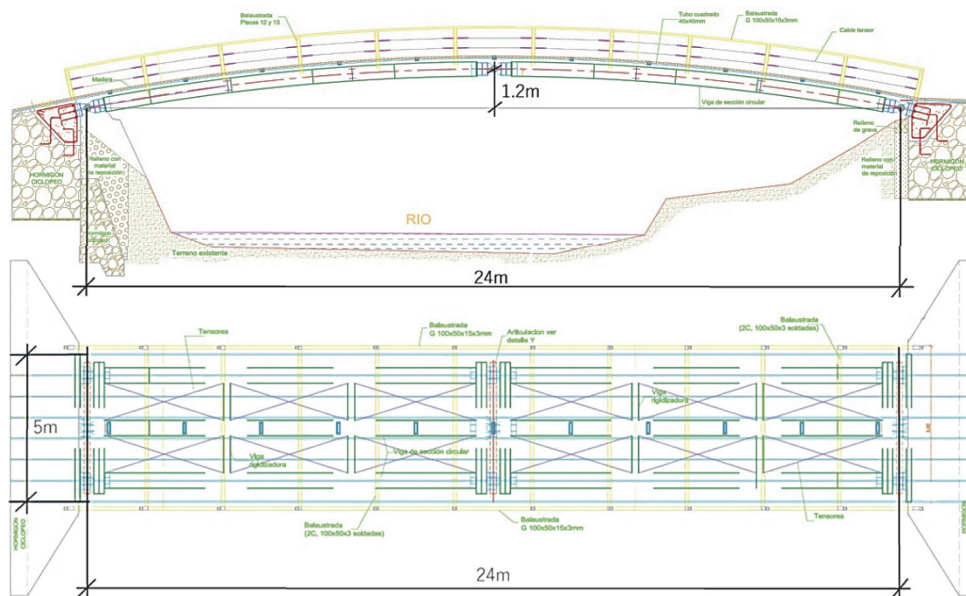

Figure 2. "Juana de Oro" footbridge [20]

Based on the overall dimensions of Juana de Oro bridge, we defined the geometry of the studied hyperbolic paraboloid shell. The defined structure is a shell with $L = 24$ m span, $B = 5$ m width, $f = 1.2$ of rise and $t = 0.1$ m thickness (Figure 3).
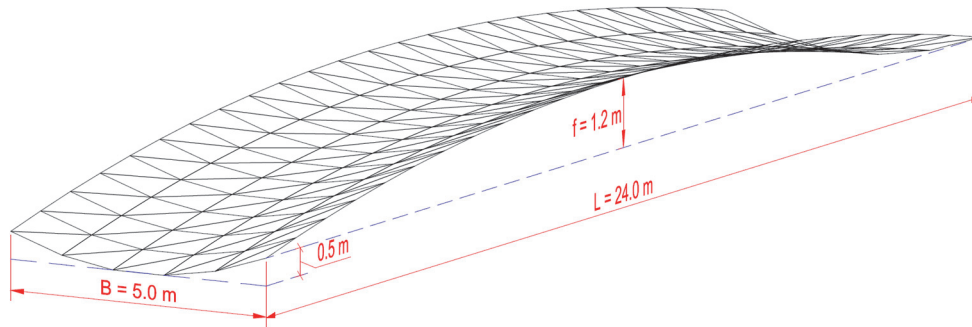

Figure 3. Overall dimensions of the studied hyperbolic paraboloid shell structure

For the defined hyperbolic paraboloid shell structure, 60 finite element models were analysed, which include the different combinations of parameters: 5 concrete strengths (28, 40, 80, 120 MPa), 3 support conditions (simple supports, fixed ends or two-hinged model, embedded ends or hingeless model), and 5 crowd load positions.

The present stress-strain study involves: 1) determination of most unfavourable loading condition for the proposed shell; 2) determination of the least efficient support conditions in terms of stresses and strains; 3) definition under which loading conditions and with which support types we will continue the research; 4) investigation of influence of the concrete strength on the stress-strain state for the selected loading condition and support type; 5) analysis of results and drawing the conclusions.

Geometry definition of the hyperbolic paraboloid (hypar) shell. A hyperbolic paraboloid is a surface whose general equation in Cartesian coordinates (x, y, z) satisfies the equation: $z = (x/a)^2 – (y/b)^2$. According to Krivoshapko & Ivanov's Encyclopedia of Analytical Surfaces [10], the explicit (canonical) equation of a hyperbolic paraboloid has the following form:

$$z = \frac{x^2}{2p} - \frac{y^2}{2q} , \ p > 0, q > 0. \tag{1}$$

The formula (1) shows that hyperbolic paraboloids can be generated by the translation of a mobile parabola $y^2 = -2qz$ along a fixed parabola $x^2 = 2pz$ or vice versa [10]. The computer model of the studied shell (Figure 3) was generated by the computational integrated system for finite element structural analysis and design SCAD++, and the system of equations (2) was obtained by the built-in SCAD++ application. In this program we have: h_0 = height of the angle point, m; h_1 = height of the inflection point along the X-axis, m; h_2 = height of the inflection point along the Y-axis, m; W = length of the plane in the X direction, m; B = length of the plane in Y direction, m (Figure 4). It should be noted that the edges of hyperbolic paraboloid can be curved or straight [21], and in our case we have defined a rectangular shape (24×5 m) on the horizontal plane projection.

$$x = (s - 0.5)W,$$

$$y = (t - 0.5)B, \tag{2}$$

$$z = h_0 + 4(h_0 - h_2)(s - 0.5)^2 + 4(h_0 - h_1)(t - 0.5)^2.$$

Live (crowd) load arrangement. In order to consider the most unfavourable position of the live load in the structure and its combination with the self-weight, we assumed the following 5 live load arrangements (Figure 5) for a pedestrian load of 4.1×10^{-3} MPa [22]:
– CV1: the crowd load occupying the entire width and half of the bridge span;
– CV2: the crowd occupying the entire width and full bridge span;
– CV3: the crowd occupying the full width and the middle third of the bridge span;
– CV4: the crowd in one lateral side (half of the width) and the entire length of the bridge;
– CV5: the crowd occupying the initial lateral side (half of the width and half of the bridge span).
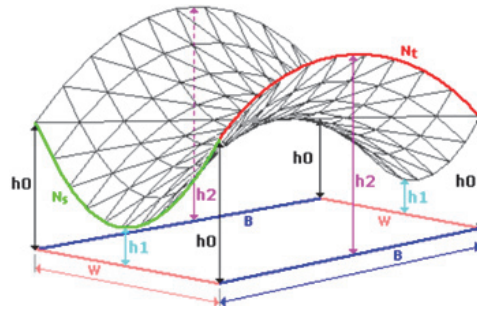
Figure 4. Geometric parameters for defining a hyperbolic paraboloid in SCAD software
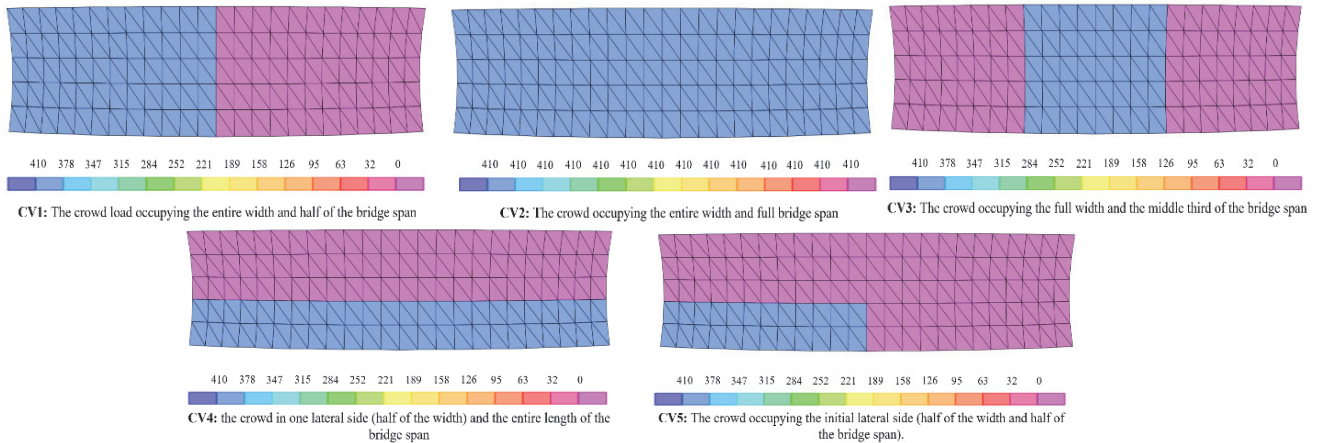

Figure 5. Live load arrangement. Live load acting on the blue areas

Compressive strength of the concrete. The investigation of the stress-strain state of the shell includes the study of the influence of different concrete strengths (28, 40, 80 and 120 MP). Since, the common practice in bridge construction in the city of Cuenca and the recommendation given in [22] suggest a concrete strength of 28 MPa, the American Concrete Institute specifies 41 MPa as the lower limit for high-resistance concrete (HRC) [23–25], and the Portland Cement Association points 120 MPa as the minimum compressive strength for ultra-high performance concrete (UHPC) [26–29], however, some authors suggest a value of 150 MPa as the minimum compressive strength limit of UHPC [30–33]. Thus, we analysed the shell for strengths of 28 and 40 MPa that correspond to a concrete of standard compressive strength, 80 MPa matches an HRC and 120 MPa corresponds to lower referred limit of UHPC.

Finite element analysis. The finite element structural analysis was performed in SAP2000 (CSI Computers & Structures, Inc.). We analysed 60 finite element models that include the following combinations of parameters: for each compressive strength (28, 40, 80, 120 MPa) were analysed 15 models that include 5 live load arrangements for the simply supported system, the same 5 load arrangements for the system with pinned ends, and the same for the model with fixed ends.

For the finite element analysis, it is necessary to define the physical and mechanical properties of analysed concrete (specific weight, modulus of elasticity and Poisson coefficient). Some recommendations about the specific weight for concretes with compressive strength less than 35 MPa suggest a value of 2320 kg/m³, instead for concretes between 35 and 105 MPa the following formula should be used [22]:

$$\gamma_c = 2240 + 2.29 f_c'. \tag{3}$$

Here γ_c = specific weight, kg/m³; f_c' = compressive strength of concrete, MPa.

In this way the concrete of 40 MPa would have a specific weight of 2332 kg/m³, and the concrete of 80 MPa a value of 2432 kg/m³. For the concrete of 120 MPa not being within the range given by the AASHTO [22] a value of 2515 kg/m³ was taken [22; 34].

The modulus of elasticity for models with compressive resistance of 28, 40 and 80 MPa was calculated based on the formula (4) which is applicable only for concretes with specific weights between 1440 and 2500 kg/m³ [22].

$$E_c = 0.043\gamma_c^{1.5}\sqrt{f_c'}. \qquad (4)$$

Here E_c = modulus of elasticity, kg/cm^2; γ_c = density of concrete, kg/m^3; f_c' = compressive strength of concrete, MPa.

For the concrete of 120 MPa a value of 459 000 kg/cm^2 (~45 900 MPa) was taken [35]. The assumed Poisson coefficient is 0.2 since no physical tests of the materials were performed [22; 36].

For the analysis of the stress-strain state, we calculated 5 load combinations in the SAP2000 software. These combinations consider the structure dead load (CM) whit each pedestrian live load in its different arrangements on the deck (CV). We replicate these load combinations for the proposed supports types and concrete strengths.

Results and discussion

The Figure 6 shows some graphical views of the stress-strain state of the models based on the finite element analysis. The Figure 7 shows the character of the normal forces in the shell.
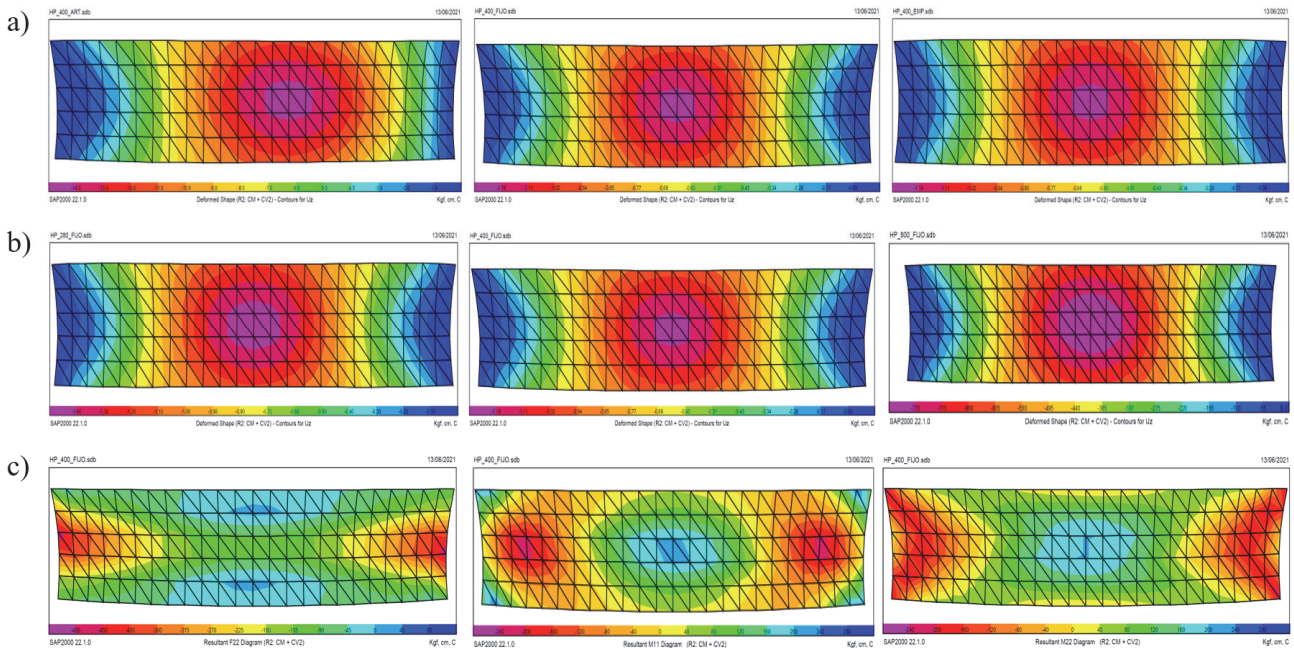

Figure 6. Comparison of deformations between different types of supports for the same concrete strength (*a*); comparison of deformations between different concrete strength but with the same type of support (*b*); internal reactions for a concrete strength of 40 MPa with fixed supports (*c*)
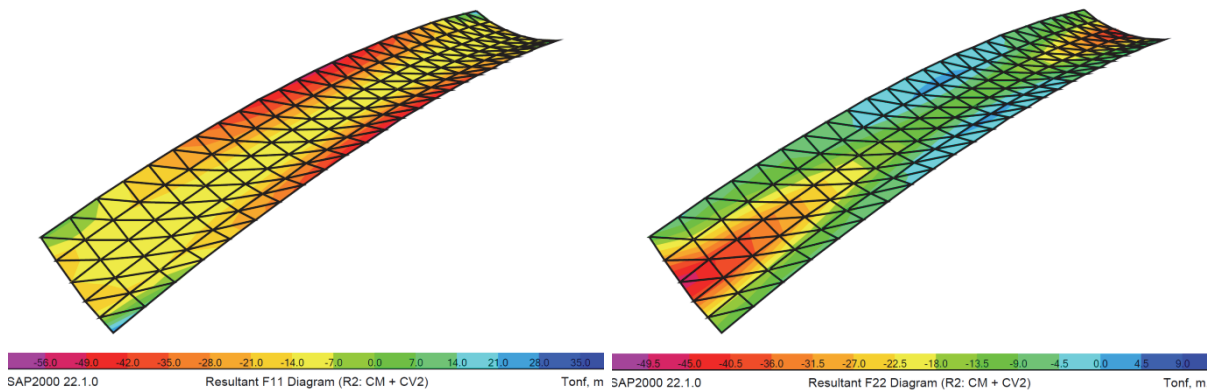

Figure 7. Character of the normal (longitudinal and transverse) forces in the shell

The results of the finite element analysis of the proposed models show that the combination named R2 and R4 (corresponding to CV2 and CV4 respectively) are the most unfavourable live load arrangement for all models regardless of the type of supports (Figure 8).
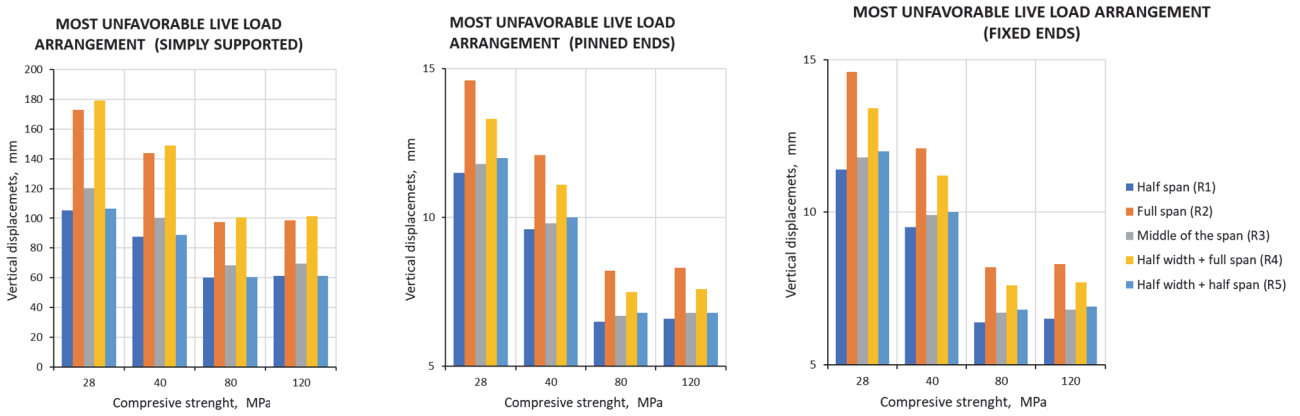
Figure 8. Influence of the live load arrangement in function of the type of supports and compressive strength of concrete
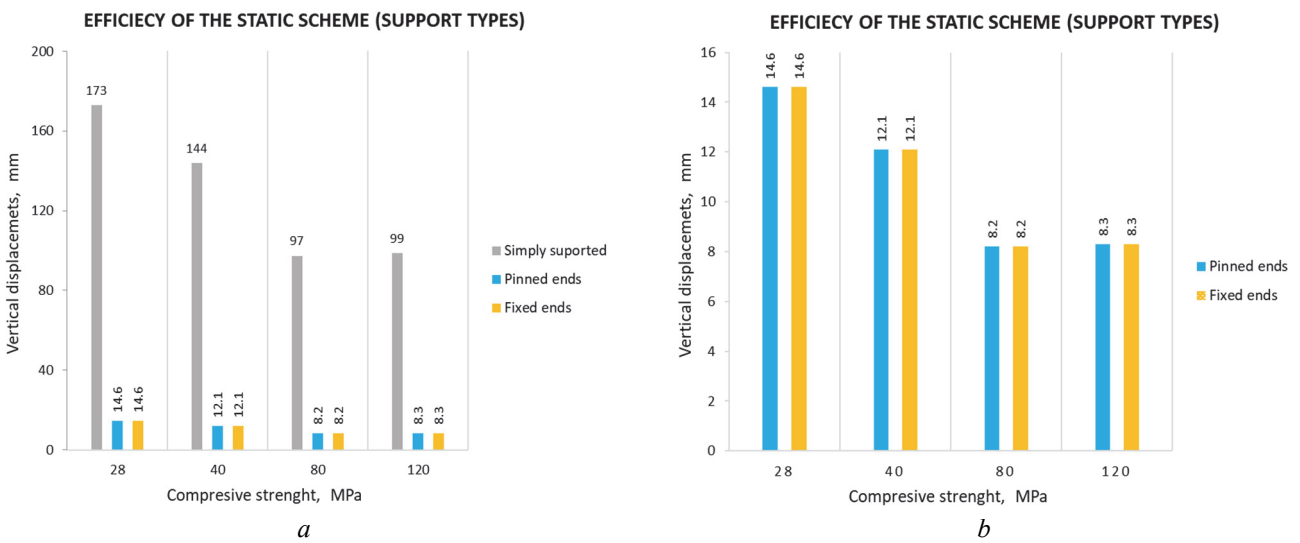

Figure 9. Influence of the support conditions. Vertical displacements by load case R2 in function of compressive strength of concrete
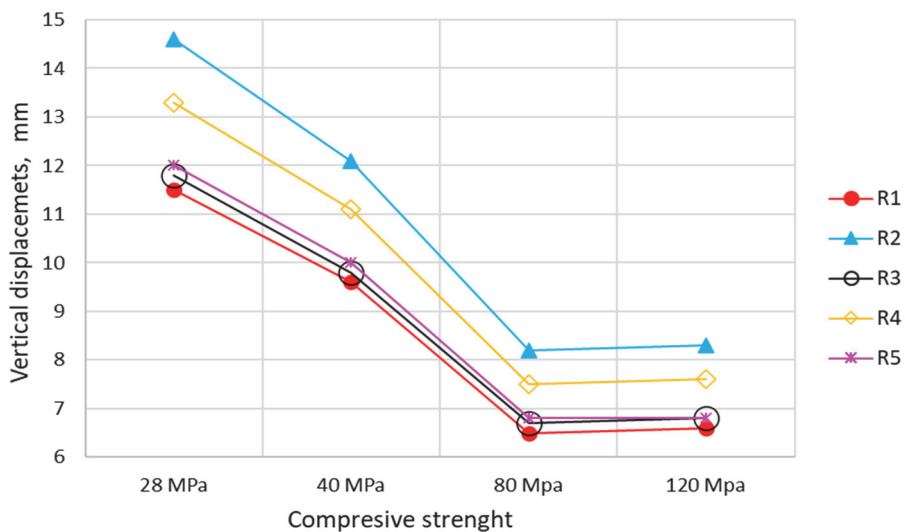

Figure 10. Influence of the compressive strength of concrete on the vertical displacements

For the defined unfavourable live load arrangement, we have studied the influence of the support conditions on the vertical displacements, the results are shown in Figure 9.

Here we can see that the simply supported condition is not viable for this type of structure, due to large displacements under the same load condition (Figure 9, *a*). Figure 9, *b* shows that vertical displacements for the pinned (hinged) ends and the fixed (embedded) ends models are the same. At the same time, it displays that the 80 MPa concrete, shows a better performance in terms of rigidity among the studied strengths.

The effect of compressive strength of the concrete was analysed for the five proposed live load arrangements. The results are shown in the Figure 10. Here we can note that the HRC (80 MPa) presents a deformational behaviour slightly better than the UHPC (120 MPa), under the same geometric parameters of the shell and live load arrangements.

In order to understand the influence of the concrete strength, we performed a stress state comparison between the pinned ends and fixed ends models under the R2 load arrangement for the 4 proposed compressive strengths of concrete. Below, in the Figures 11–13, we show the graphs that summarise the results of the stress state investigation.

In these graphs we can see that the maximum internal reactions in the shell with pinned supports are lower than in the ones with fixed supports regardless of the analysed concrete strength.

Further, the structural performance of the "hypar" shell was analysed as a function of the compressive strength of the concrete. In this research a point of balance between stresses and strains was determined according to the strength of the concrete. The graph below shows that, as the concrete strength increases, the internal reactions also increase, while the deformations decrease. However, the deformations stabilise at strengths close to or above 80 MPa. This analysis shows that the better relation between strains and stresses is for a concrete next to 80 MPa of compressive strength (Figure 14).
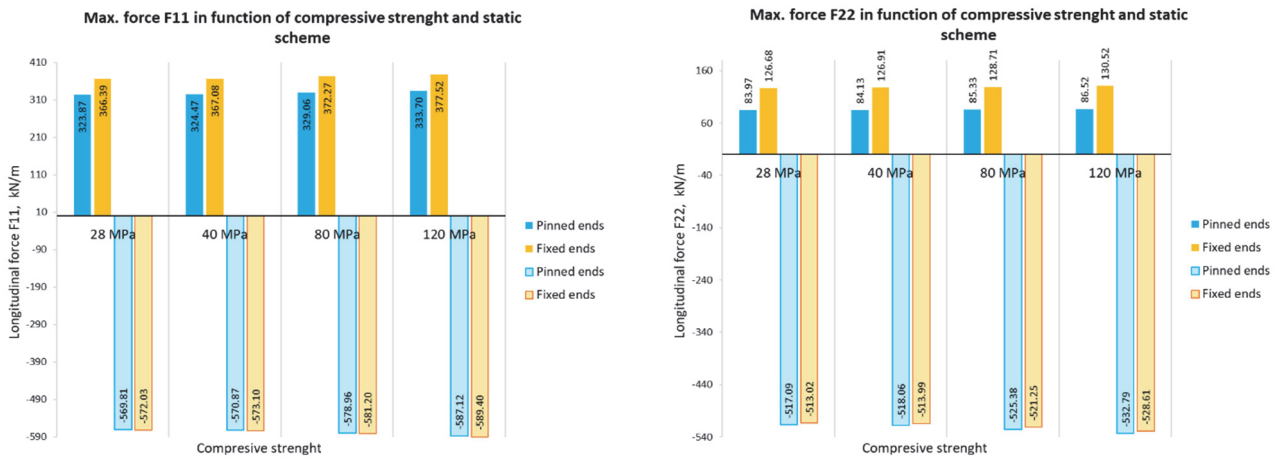

Figure 11. Maximum internal force along the longitudinal and transverse local axes of the shell
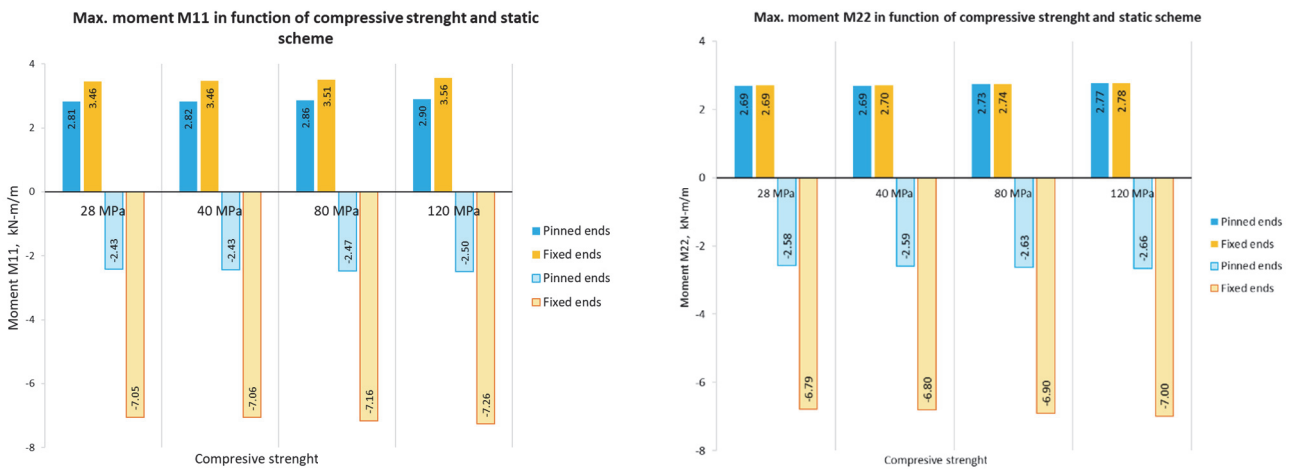

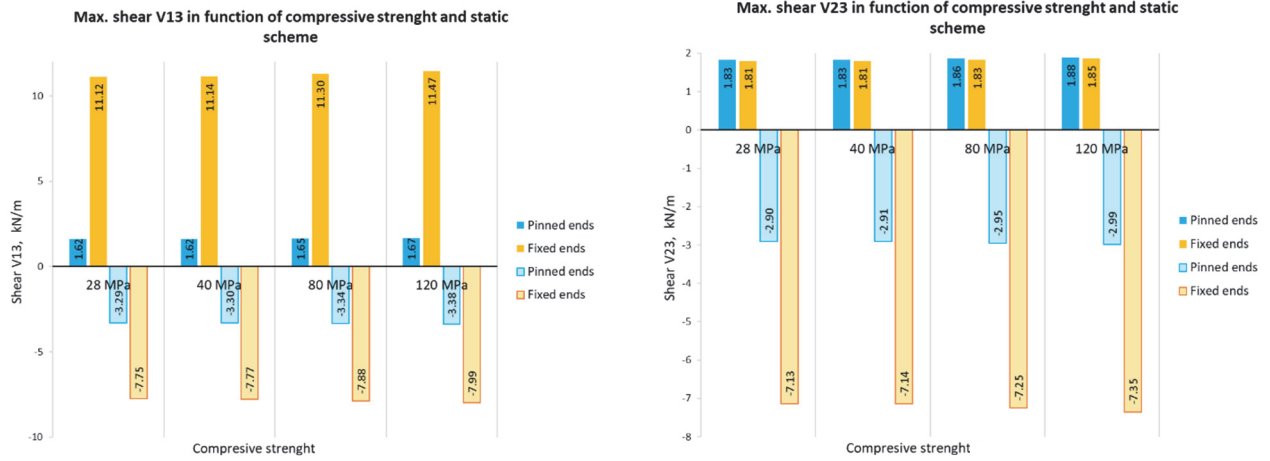**Figure 12.** Maximum bending moment along the local axes of the shell
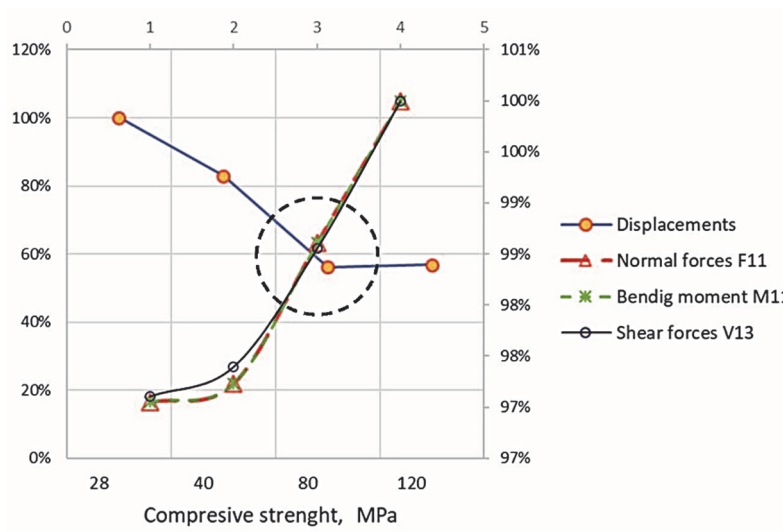
Figure 13. Maximum shear forces

Figure 14. Influence of the compressive strength of concrete on the structural performance (stress-strain state) of the proposed hyperbolic paraboloid shell
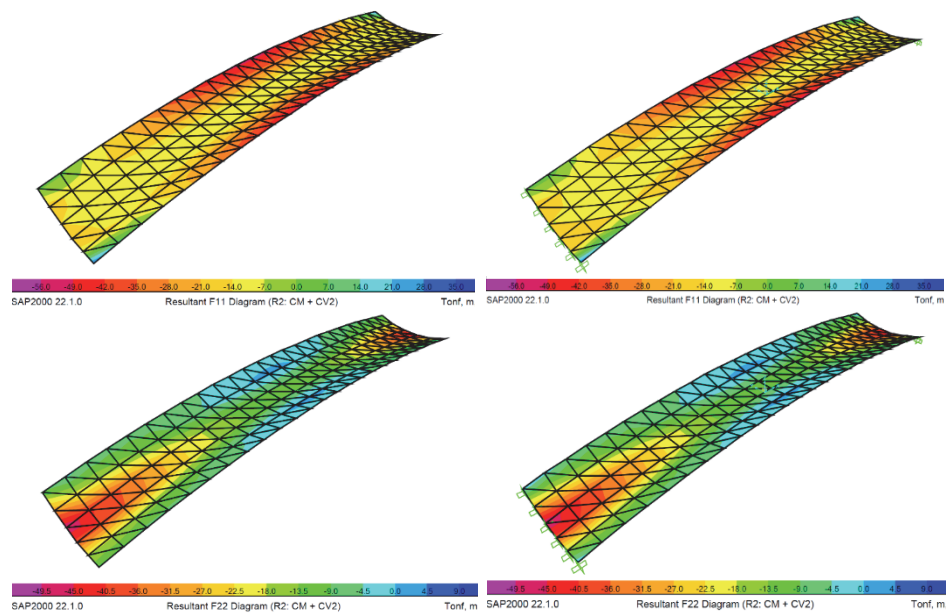

Figure 15. Distribution of normal forces F11 and F22
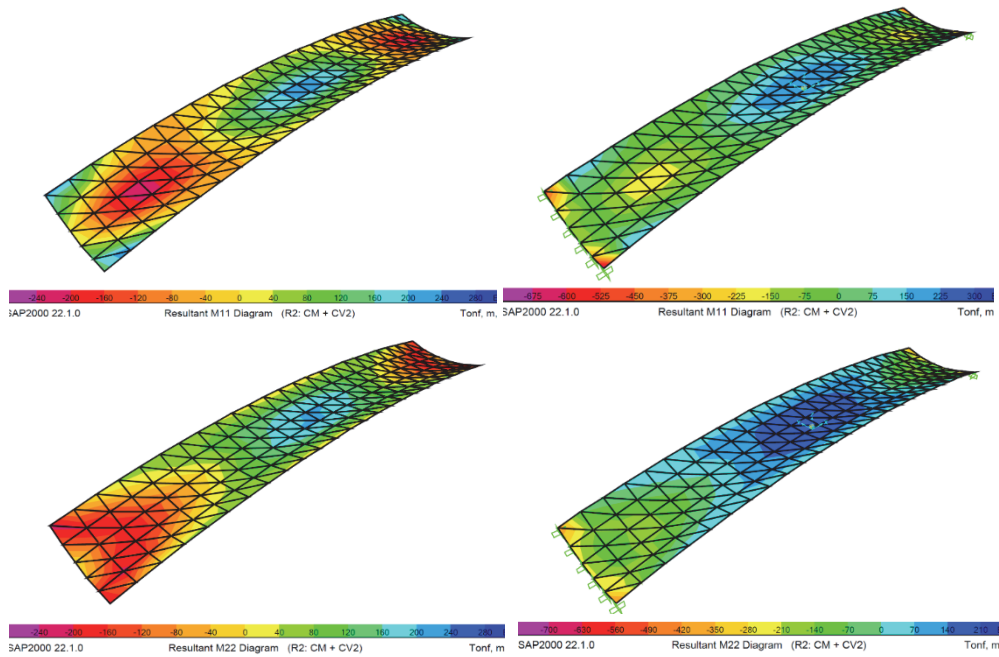
Figure 16. Distribution of bending moments M11 and M22
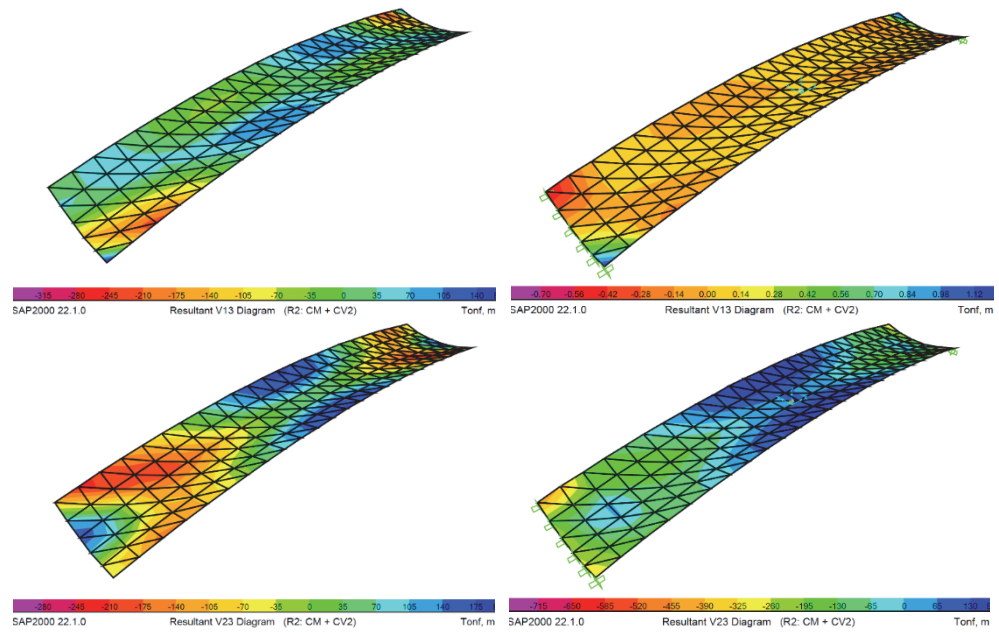
Figure 17. Distribution of shear forces V13 and V23

The Figures 15–17 show the character of the stress state of the shell studied with 80 MPa concrete, both for the case of hinged supports (right pictures) and for the case of embedded supports (left pictures).

Conclusion

The purely geometrical shape of the hyperbolic paraboloid is relatively easy to work with, both from structural analysis and design viewpoint. However, the effects of the bending stresses that are generated for the given geometry must be considered. These bending stresses should be dealt with rationally by adjusting the curvatures of the shell instead of increasing the cross-section [37].

In this investigation, the assessment of the static structural behaviour of a hyperbolic paraboloid shell was performed in order to evaluate the possibilities of application of this analytical surface as a shell-shaped footbridge where the shell is both the load-bearing element and the walking surface. In terms of rigidity was deter-

mined that the pinned (hinged) supports and fixed (embedded) supports give almost equal displacement magnitudes (Figure 9, *b*). The FEA analysis shows a vertical displacement of 8.2 mm for the 80 MPa model and 8.3 mm for the 120 MPa model. However, in terms of stresses, the pinned supports shown better behaviour than fixed ones. The normal tensile forces *F11* along the longitudinal axis for the pinned supports are 11.61% less than the fixed supports. The normal compressive forces *F11* along the longitudinal axis for the pinned supports are 0.39% less than the fixed supports. The normal tensile forces *F22* along the transversal axis for the pinned supports are 33.71% less than the fixed supports. The normal compressive forces *F22* along the transverse axis for the pinned supports are 0.79% greater than the fixed supports. The maximum magnitude of bending moment *M11* along the longitudinal axis for the pinned supports is 65.54% less than the fixed supports. The maximum magnitude of bending moment M*22* along the longitudinal axis for the pinned supports is 61.95% less than the fixed supports. The maximum shear forces *V13* for the pinned supports are 85.45% less than the fixed supports. The maximum shear forces *V23* for the pinned supports are 59.26% less than the fixed supports.

The study of the influence of the compressive strength of the concrete on the one hand shows that the HRC (80 MPa) shell has 43.49% less displacement than the normal resistance concrete (28 MPa), 32.16% less than the 40 MPa, and even 1.37% less than the UHPC (120 MPa). But on the other hand, it shows an increase of internal reactions as follows: for the 40 MPa concrete the internal reactions increase 0.18% compared to the 28 MPa; for the 80 MPa concrete the internal reactions increase 1.41% compared to the 40 MPa; and for the 120 MPa the internal reactions are 1.36% greater than for the 80 MPa concrete.

These results show that, in terms of maximum stresses, the hyperbolic paraboloid with pinned (two-hinged) supports is the more adequate static scheme for the proposed anticlastic shell, while a concrete with compressive strength between 40 and 80 MPa provides the best structural performance. However, it could be observed that the model with fixed (hingeless) supports shows a most uniform stress distribution. Later the research will continue on the 40 and 80 MPa pinned-support (two-hinged) and fixed-support (hingeless) shell. In future articles we will determine the structural behaviour under static and dynamic actions, including seismic loads. We will revise the shell curvatures to optimise the structural behaviour, study the influence of the shell thickness on the UHPC alternative. Also, we will review the issues about the local stiffness as well as the need for the addition of edge beams and study its effects, about the reinforcement of the shell (type of reinforcement, steel strength, diameter, spacing) and the intensity of the reinforcement in the different zones depending on the stress-strain state.

References

1. Bradshaw R., Campbell D., Gargari M., Mirrniran A., Tripeny P. Special structures: past, present, and future. *J. Struct. Eng.* 2002;128(6):691–709. http://dx.doi.org/10.1061/(asce)0733-9445(2002)128:6(691)

2. Ramm E., Mehlhorn G. On shape finding methods and ultimate load analyses of reinforced concrete shells. *Eng. Struct.* 1991;13(2):178–198. http://dx.doi.org/10.1016/0141-0296(91)90050-M

3. Aleshina O., Cajamarca D., Barbecho J. Numerical comparative analysis of a thin-shell spatial structure for the Candela's Cosmic Rays Pavilion. *Adv. Astronaut. Sci.* 2021;174:741–752.

4. Pérez-Peraza J. Reminiscences of cosmic ray research in Mexico. *Adv. Sp. Res.* 2009;44(10):1215–1220. http://dx.doi.org/10.1016/j.asr.2008.11.031

5. Minor A. Up-and-down journeys: the making of Latin America's uniqueness for the study of cosmic rays. *Centaurus.* 2020;1–23. http://dx.doi.org/10.1111/1600-0498.12335

6. Mendoza M. Felix Candela's first European Project: The John Lewis Warehouse, Stevenage New Town. *Archit. Res. Q.* 2015;19(2):149–60. http://dx.doi.org/10.1017/S1359135515000251

7. Krivoshapko S.N., Hyeng C.A.B., Mamieva I.A. Chronology of erection of the earliest reinforced concrete shells. *Int. J. Recent Res. Appl. Stud.* 2014;18(2):95–108.

8. Krivoshapko S.N., Mamieva I.A. *Analytical surfaces in the architecture of buildings, structures and components.* Moscow: LIBROKOM Publ.; 2011. (In Russ.)

9. Kourkoutas V. *Parametric form finding in contemporary architecture Vassilis Kourkoutas.* Vienna: Technische Universität Wien; 2007.

10. Krivoshapko S.N., Ivanov V.N. *Encyclopedia of analytical surfaces* Switzerland: Springer International Publishing AG; 2015. http://dx.doi.org/10.1007/978-3-319-11773-7

11. Farshad M. Design of hyperbolic paraboloid shells. In: *Design and Analysis of Shell Structures.* Switzerland: Springer-Science+Business Media, B.V.; 1992. p. 215–247.

12. Oliva Quecedo J., Antolin Sanchez P., Cámara Casado A., Goicolea Ruigómez J.M. Finite element model analysis of works authored by Felix Candela. *Hormigón y Acero.* 2011;(1):61–76.

13. Rippmann M. *Funicular shell design geometric approaches to form finding and fabrication of discrete funicular structures.* PhD Thesis. Zurich; 2016.

14. Bischoff M., Ramm E., Irslinger J. Models and finite elements for thin-walled structures. In: *Encyclopedia of Computational Mechanics Second Edition.* John Wiley & Sons, Ltd.; 2017. http://dx.doi.org/10.1002/9781119176817.ecm2026

15. Marmo F., Demartino C., Candela G., Sulpizio C., Briseghella B., Spagnuolo R., et al. On the form of the Musmeci's bridge over the Basento river. *Eng. Struct.* 2019;191(May):658–73. http://dx.doi.org/10.1016/j.engstruct.2019.04.069

16. Fenu L., Congiu E., Lavorato D., Briseghella B., Marano G.C. Curved footbridges supported by a shell obtained through thrust network analysis. *J. Traffic Transp. Eng. (English Ed.)* 2019;6(1):65–75. http://dx.doi.org/10.1016/j.jtte.2018.10.007

17. Fenu L., Congiu E., Marano G.C., Briseghella B. Shell-supported footbridges. *Curved Layer Struct.* 2020;7(2):199–214. http://dx.doi.org/10.1515/cls-2020-0017

18. Peiretti H.C., Martín J.R., Delgado J.S., Matadero and invernadero shell footbridges over the Manzanero River in Madrid. *Rev. Obras. Publicas.* 2011;158(3520):39–50.

19. McIntyre J. Outokumpu: building bridges to span over distance and time. *Stainless Steel World.* 2019;(137):2–3.

20. Zeas Guzman K. *Los puentes del Centro Histórico de Cuenca.* Universidad de Cuenca; 2013.

21. Saltik E., Alacam S. Experiments for design and optimization of thin shell structures. *ATI 2020: "Smart Buildings, Smart Cities" Proceedings.* Izmir: Yaşar University; 2020. p. 76–90.

22. American Association of State Highway and Transportation Officials. *AASHTO LRFD Bridge Design Specifications.* 8th ed. Washington D.C.; 2017 p. 1881.

23. ACI 363R-92. *State-of-the-art report on high-strength concrete* (vol. 92). ACI Committee 363. American Concrete Institute; 1992.

24. Razvi S.R., Saatcioglu M. Strength and deformability of confined high-strength concrete columns. *ACI Struct. J.* 1994;91(6):678–696.

25. Sheikh S.A., Shah D.V., Khoury S.S. Confinement of high-strength concrete columns. *ACI Struct. J.* 1994;91(1):100–111.

26. Maten R.N. ter *Ultra high performance concrete in large span shell structure*s. Delft: Delft University of Technology; 2011.

27. Perry V., Zakariasen D. First use of ultra-high performance concrete for an innovative train station canopy. *Concrete Technology Today – Portland Cement Association.* 2004;25(2):1–7.

28. Walraven J.C. Designing with ultra high strength concrete: basics, potential and perspectives. In: Schmidt M., Fehling E., Geisenhansluke C. (eds.) *Proceedings of the International Symposium on Ultra-High Performance Concrete.* Kassel: Die Deutsche Bibliothek; 2004. p. 853–864.

29. Ramesh M.N., Teichmann T. Ultra high performance concrete: sustainable and cost effective. B2B Purchase. Mumbai; 2016. Available from https://b2bpurchase.com/ultra-high-performance-concrete-sustainable-and-cost-effective/ (accessed: 02.04.2021).

30. Azmee N.M., Shafiq N. Ultra-high performance concrete: from fundamental to applications. *Case Stud. Constr. Mater.* 2018;9:e00197. http://dx.doi.org/10.1016/j.cscm.2018.e00197

31. Sarmiento P.A., Torres B., Ruiz D.M., Alvarado Y.A., Gasch I., Machuca A.F. Cyclic behavior of ultra-high performance fiber reinforced concrete beam-column joint. *Struct. Concrete.* 2019;20:348–360. http://dx.doi.org/10.1002/suco.201800025

32. Shafieifar M., Farzad M., Azizinamini A. Experimental and numerical study on mechanical properties of ultra high performance concrete (UHPC). *Constr. Build. Mater.* 2017;156:402–411. http://dx.doi.org/10.1016/j.conbuildmat.2017.08.170

33. Dingqiang F., Wenjing T., Dandian F., Jiahao C., Rui Y., Kaiquan Z. Development and applications of ultra-high performance concrete in bridge engineering. *IOP Conf. Ser. Earth Environ. Sci.* 2018;189:22038. http://dx.doi.org/10.1088/1755-1315/189/2/022038

34. Bahr O., Schaumann P., Bollen B., Bracke J. Young's modulus and Poisson's ratio of concrete at high temperatures: experimental investigations. *Mater. Des.* 2013;45:421–429. http://dx.doi.org/10.1016/j.matdes.2012.07.070

35. Mostofinejad D., Nozhati M D. Prediction of the modulus of elasticity of high strength concrete. *Iranian Journal of Science and Technology Transaction B: Engineering.* 2005;29(B3):311–321.

36. Chen H.J., Yu Y.L., Tang C.W. Mechanical properties of ultra-high performance concrete before and after exposure to high temperatures. *Materials (Basel).* 2020;13(3):1–17. http://dx.doi.org/10.3390/ma13030770

37. Ohmori H., Yamamoto K. Shape optimization of shell and spatial structure for specified stress distribution. *Mem. Sch. Eng. Nagoya Univ. Japan.* 1998;50(1):1–32.